



Geophysical investigation of structural involvement in collapse dolines belong Abda region, western Morocco

Ahmed Fadili¹ · Othmane Boualla² · Saliha Najib³ · Abdelhadi Makan⁴ · Khalid Mehdi^{3,5} · Mohammed Bouzerda⁵ · Hasna Bouftou⁵ · Issam Mehdi⁶ · Abdel-Ali Kharis¹ · Marouane Achnoui⁷ · Boubker Belkaid⁷ · Bendahhou Zourarah⁵

Received: 20 September 2023 / Accepted: 8 January 2024

© The Author(s) under exclusive licence to Institute of Geophysics, Polish Academy of Sciences & Polish Academy of Sciences 2024

Abstract

The Abda region in western Morocco is currently grappling with unpredictable hazards related to the occurrence of collapse dolines. These hazards have inflicted notable harm on the local population, infrastructure, and agricultural lands, causing substantial environmental repercussions. Given the gravity of this situation, the present research systematically investigates the processes and mechanisms of the genesis of collapse dolines within the study area, employing an integrated approach that combines fieldwork, geological survey, and geophysical techniques. More than thirty collapse dolines were identified, characterized by a prevailing NE–SW orientation and a close alignment with major faults. Field observations provided essential insights into doline composition and susceptibility, with Quaternary formations exhibiting the highest vulnerability, followed by the Plio-quaternary and evaporitic complex formations. The integration of electrical resistivity tomography (ERT) and Seismic refraction tomography (SRT) techniques yielded further geological understanding. The results highlighted distinct discontinuities in both ERT and SRT profiles, confirming the presence of faults and fractures linked to collapse dolines. The combination of these geophysical findings with lineament analysis from satellite data further revealed a correlation between doline alignments and major faults. Overall, the susceptibility of the Abda region to collapse events is driven by a combination of geological composition, structural elements, and hydrological patterns. These factors collectively amplify the risk of surface subsidence due to continual erosion and dissolution processes. In light of these insights, it is imperative to address the potential risks posed by collapse dolines through comprehensive mapping and meticulous delineation of the influential factors to ensure the safety and stability of vulnerable regions.

Keywords Collapse dolines · Electric resistivity tomography · Seismic refraction tomography · Abda region · Morocco

Edited by Assoc. Prof. Dr. Bogdan Mihai Niculescu (ASSOCIATE EDITOR) / Prof. Gabriela Fernández Viejo (CO-EDITOR-IN-CHIEF).

✉ Ahmed Fadili
fadiliahmed@gmail.com; a.fadili@uiz.ac.ma

✉ Othmane Boualla
bouallaothmane@gmail.com; o.boualla@uiz.ac.ma

¹ Polydisciplinary Faculty of Ouarzazate (FPO), Ibnou Zohr University, 45000 Ouarzazate, Morocco

² Geosciences, Environment, and Geomatic Laboratory, Team of Geomatic and Geophysics, Department of Geology, Faculty of Sciences, Ibnou Zohr University, B.P. 8106, Agadir, Morocco

³ Polydisciplinary Faculty of Khouribga (FPK), Sultan Moulay Slimane University, 25000 Khouribga, Morocco

⁴ Team of Environmental Management and Civil Engineering (GEGC), National School of Applied Sciences (ENSAH), Abdelmalek Essaadi University, Tetouan, Morocco

⁵ Marine Geosciences and Soil Sciences Laboratory (LGMSS), Department of Geology, Faculty of Sciences, Chouaib Doukkali University, El Jadida, Morocco

⁶ Mohammadia School of Engineering, Laboratory of Geotechnics, Geophysics, Engineering and Environmental Geology (L3GE), University Med V, Rabat, Morocco

⁷ Ocean Association of Speleology, Safi, Morocco

Introduction

Regions characterized by carbonated formations frequently harbor numerous karstic structures, including cavities and fractures (Amanatidou et al. 2022; Boualla et al. 2021). These structures increase the complexity of the underlying systems and are often associated with environmental and geotechnical hazards for infrastructure and agricultural lands (Carollo et al. 2020; Boualla et al. 2021; Amanatidou et al. 2022). Several research studies have pointed out that the existence of such structures can induce ground instability, potentially resulting in the sudden and unexpected collapse of the land surface (De Giorgi and Leucci 2014; Boualla et al. 2021). In this context, numerous documented cases worldwide have highlighted the widespread impact of collapse phenomena in regions with similar geological characteristics. (Gutiérrez Elorza 2008; Metwaly and AlFouzan 2013; Boualla et al. 2021). For instance, in Spain, Gómez-Ortiz and Martín-Crespo (2012) conducted a risk assessment for collapse sinkholes using a combination of ground-penetrating radar (GPR) and electrical resistivity tomography (ERT) techniques. Their findings revealed a strong correlation between the risk of collapse and the existence of underground cavities, with significant impacts on various anthropic structures, including a highway and agricultural fields. In west-central Florida, Oliver-Cabrera et al. (2020) claimed that the formation of sinkholes can be attributed to the movement of rocks or sediments into voids created by rock dissolution. They further asserted that the increasing frequency of their occurrence is closely tied to the accelerated utilization of both groundwater and land resources in the region. In a recent study, Khoshlahjeh Azar et al. (2021) underscored that the emergence of several sinkholes in Iranian plains is due to the distinctive properties of underground soil layers and the severe depletion of groundwater. In their effort to address the associated hazards, the authors employed the Persistent Scatterer Interferometry (PS-InSAR) method to investigate the deformation behavior preceding sinkhole formation. In Italy, some researchers have effectively generated a sinkhole risk zoning map, serving as an early warning system to inform urban planning and facilitate the development of robust risk management strategies (Intrieri et al. 2023).

Like many regions susceptible to land collapses, the Abda region in western Morocco (Fig. 1) is characterized by the dominance of karstic formations and structures (Boualla 2016; Bouzerda et al. 2020; Boualla et al. 2021), already featuring many collapse dolines on the ground surface. When assessing susceptibility to collapse dolines, Boualla et al. (2016) demonstrated that the Abda region, including the area under study, exhibits high to very

high susceptibility levels. These researchers attributed the occurrence of these collapses primarily to lithology and likely the presence of major faults. Similarly, in their investigations of collapse susceptibility in the Sahel Doukala region north of the study area, Bouzerda et al. (2020) demonstrated that the functioning of the karstic system is mainly governed by underground flows and major faults. Not far from the area under study, Boualla et al. (2021) employed geophysical surveys using ERT coupled with field inventory to identify the diverse mechanisms contributing to the occurrence of collapses in the Moul El Bergui zone (Fig. 1). They also established that structural and tectonic factors participate as predisposing elements in the development of collapse dolines. According to Weisrock and Lunski (1987), the collapse dolines could be linked to dissolution phenomena affecting the deep gypseous karst formations of the Upper Jurassic age. However, the dissolution process could also affect the limestone formations, which constitute a large portion of the area (Roch 1950; Gigout 1951). Weisrock and Lunski (1987) added that dissolution not only occurs in gypsum and anhydrite formations but also affects the overlying limestone formations.

The existing literature affirms that tectonic structures, such as folds and faults (Pothérat et al. 1999), along with drainage patterns within karstic aquifers (Williams 2003; Gilli et al. 2012), play a crucial role in determining the relative distribution of dolines. While previous studies conducted in the Abda region consistently hints at the potential involvement of major faults in the occurrence of dolines, comprehensive fault mapping remains an unexplored area of research. In addition, the direct implication of faults in the genesis of collapse dolines is yet to be confirmed, leaving a significant knowledge gap concerning the precise mechanisms driving their formation. Notably, the karstic structure and collapse dolines in this region typically follow preferred orientations along specific axes (Boualla 2016; Boualla et al. 2021). Consequently, mapping potential fault axes could yield further insights into the mechanisms governing these structures.

According to literature records, geophysical investigations seem to be reliable means to achieve these objectives. However, selecting the most suitable geophysical technique for mapping underground faults is far from straightforward, typically hinging on the geological characteristics of the site (Imposa et al. 2018). Notably, several authors have showcased the effectiveness of both ERT and seismic refraction tomography (SRT) when applied to various geological contexts (Ammar and Kamal 2018; Rizzo et al. 2019; Alqahtani et al. 2021). These techniques emerge as the most frequently employed methods for gathering information about karst structures and geometries (Cardarelli et al. 2010; Imposa et al. 2018; Ducut et al. 2022; Boualla et al. 2021; Guedes et al. 2023). The SRT method has yielded particularly

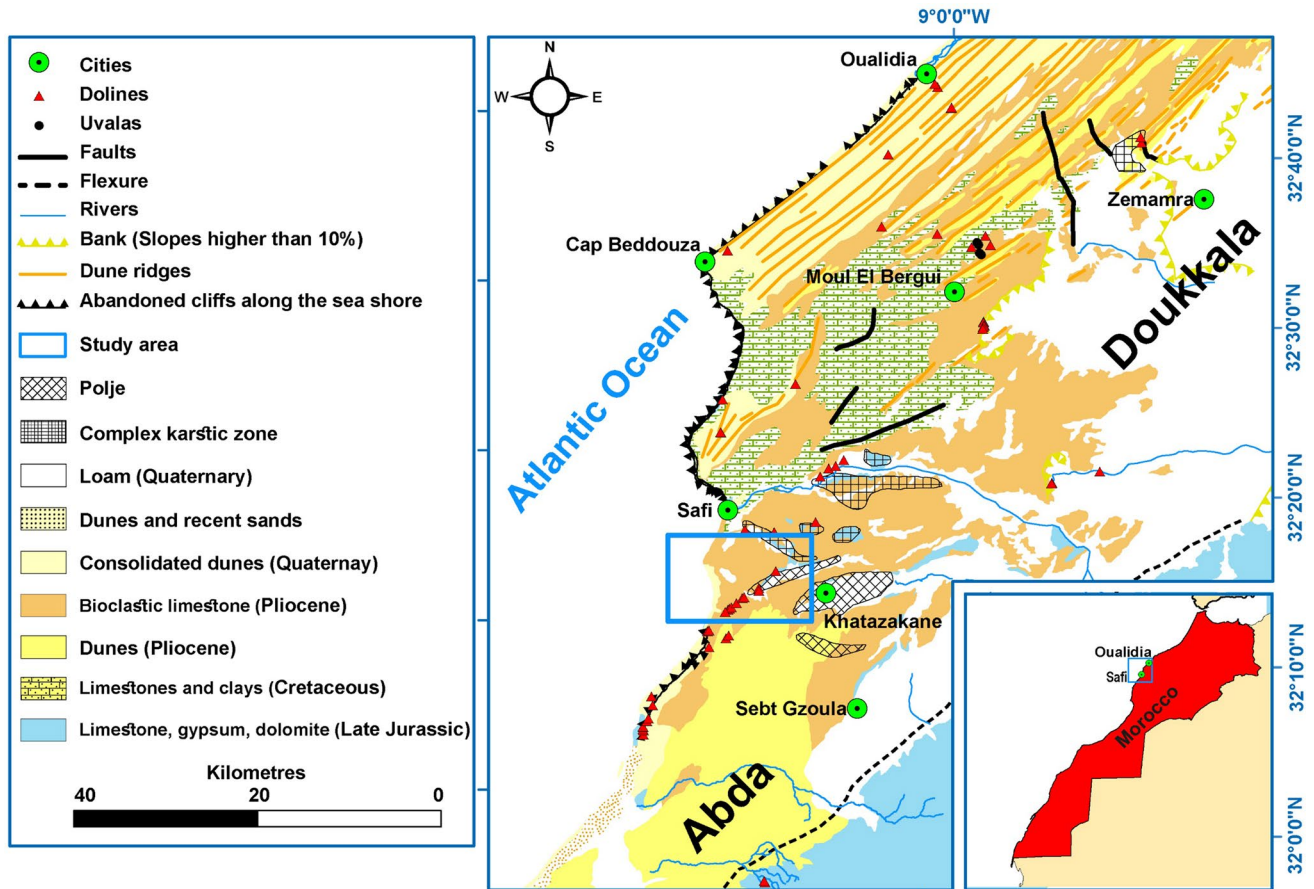


Fig. 1 Geological and geomorphological map of the study area modified from Ferré and Ruhard (1975)

valuable findings in geological studies, especially within karstic environments (Cardarelli et al. 2014; Olivier et al. 2018; Imposa et al. 2018; Guedes et al. 2023). Additionally, the ERT method has been demonstrated to be equally effective in mapping karstic structures across a wide variety of geological contexts (Carollo et al. 2020; Boualla et al. 2021; Alqahtani et al. 2021; Amanatidou et al. 2022).

In harmony with previous research and aiming to enhance our understanding of the mechanisms and processes involved in collapse doline formation, we conducted a comprehensive geophysical survey using ERT and SRT profiles in the study area. These profiles were strategically established in close proximity and perpendicular to the alignment of the collapse dolines. The primary objectives of the present study include characterizing the karstic features within the study area, identifying faults and fractures that could influence the initiation and alignment of these collapse dolines, and elucidating the fundamental mechanisms governing their genesis. The study stands out due to its innovative approach, which integrates ERT and SRT data to comprehensively assess karstic features. This approach not only facilitates mapping but also confirms the presence of faults, thus validating

their involvement in ground movements. Additionally, this research builds upon prior investigations carried out in different geological and geomorphological contexts, contributing to ongoing discussions. Finally, the insights derived from this study hold significant potential for informed regional planning in areas susceptible to collapse events.

Materials and methods

Study area description

The area under study belongs to the Abda region, an integral part of the western Mesetian domain of Morocco (Fig. 1). From the geological point of view, this area predominantly consists of formations attributed to the Jurassic, Cretaceous, and marine Pliocene periods. Notably, Gigout (1951) described the coastal section of the region, which is marked by a cliff, as featuring a limestone bedrock, followed by several meters of greenish marl and fine limestone, and finally calcareous sand with low clay content. Choubert and Faure-Muret (1962) elaborated

that the upper Pliocene is formed by molasses; while, the marine Pliocene is composed of Villafranchian consolidated dunes. Witam (1988) further divided the geology of the region into two parts: the Upper Jurassic evaporitic complex and the Plio-Villafranchian calcareous sandstone.

The study area is known for its complex karstic system (Roch 1950; Gigout 1951). Weisrock and Lunski (1987) revealed the existence of two superimposed karsts: the profound Upper Jurassic karst and the superficial karst originating from Plio-quaternary formations. These karstic features are visible on the surface in the form of collapse dolines, uvalas, and poljes (Figs. 1 and 2). Importantly, these structures generally align along three main directions: N170-N195, N040-N070, and N080-N115, which are probably due to tectonic influences (Weisrock and Lunski 1987). The first direction corresponds to the Hercynian orogeny; while, the latter two correspond to the Alpine orogeny.

Geophysical survey and data acquisition

The main objective of this study is to map potential faults and karstic structures, aiming to confirm their involvement

in the ground collapse within the study area. To achieve this objective, geophysical profiles were established in proximity to the dolines and perpendicular to their alignment across four distinct zones (Fig. 2). Moreover, the chosen positions were oriented perpendicularly to the expected path of the faults or fractures linking the collapse dolines. In the field, the SRT profiles were set to cross and overlap at a certain distance with the ERT profiles. Overall, four ERT and four SRT profiles were executed along a general N-S direction between the collapse dolines, as depicted in Fig. 2.

ERT measurements were carried out in field using the Syscal junior 72-Swich system provided by IRIS instruments. Each profile comprised 72 electrodes spaced at 5-m intervals, connected through a multi-electrode cable, with a total length of 355 m. The electrical array used in this study was the Wenner–Schlumberger array, providing a prospecting depth of around 70 m. The acquired apparent resistivity pseudo-sections were inverted using Res2DInv software (Loke 2014). The inversion process followed the least squares optimization method with a smoothness constraint (Loke and Barker 1996). A total of 6 inversions were performed, yielding final relative root mean square errors

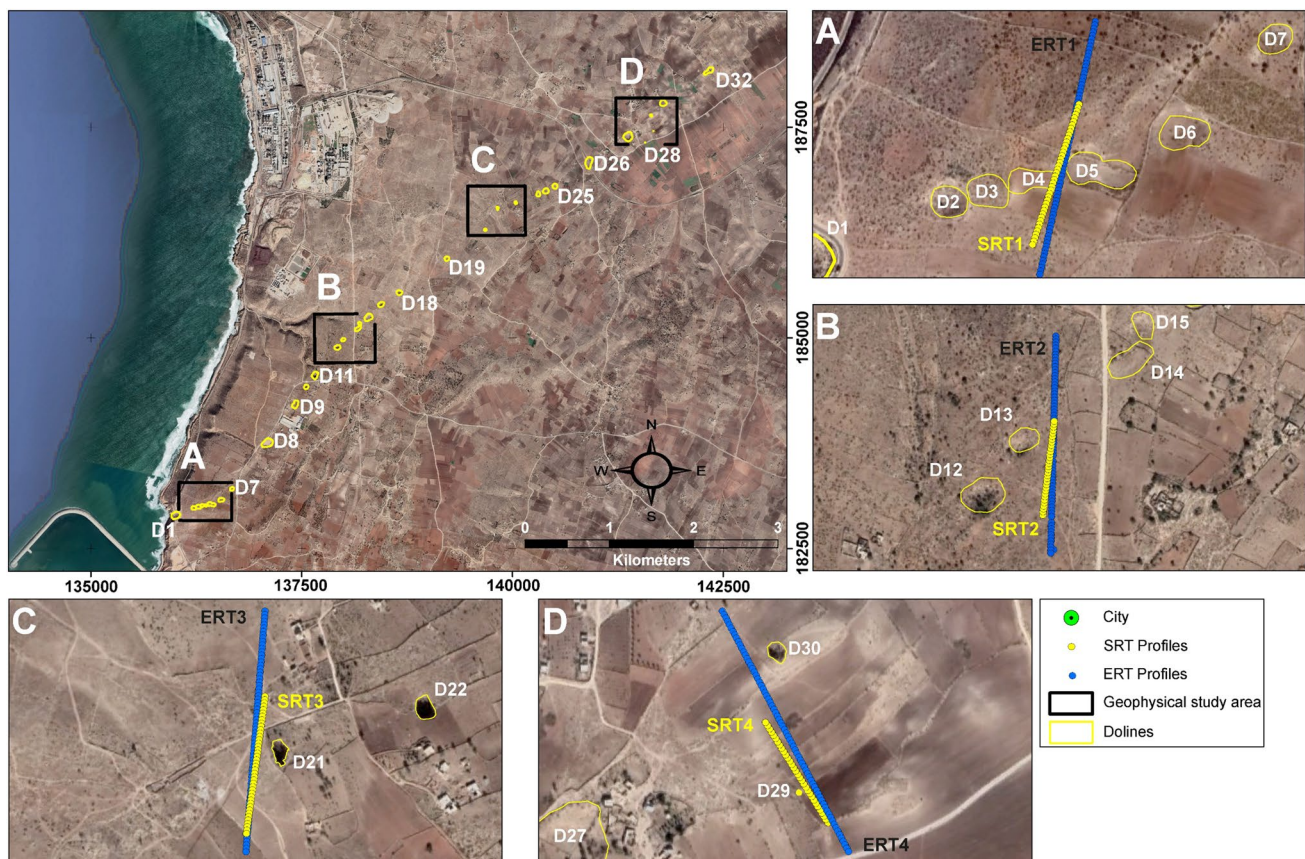


Fig. 2 Aerial photographs depicting doline locations and geophysical profile positions in the study area

of 2.8%, 8.9%, 2.3%, and 5.0% for ERT1, ERT2, ERT3, and ERT4, respectively.

Seismic data were acquired with a Smartseis st3000 seismometer, using a 5 kg hammer and steel plate as seismic source. Roll-along profiles were conducted using a set of 12 vertical geophones with a frequency response of 14 Hz at 5-m intervals. The length of each profile ranged from 155 to 255 m. Within each profile section, a total of 11 shotpoints were positioned between geophones, complemented by an additional 6 shotpoints at distances of -20 , -10 , -5 , 60 , 65 , and 75 m from the first and last geophones, as presented in Fig. 3. This shot distribution aimed at achieving high-resolution seismic ray coverage. The first arrivals defined for each shot and the travel time tomography were produced using SeisImager software. An illustrative data acquisition example along SRT2 profile is shown in Fig. 4. In total, 10 iterations were defined for the reconstruction of the velocity models after data inversions. At the end of the last iteration, the resulting relative root mean square errors for SRT1, SRT2, SRT3, and SRT4 profiles were 5.2%, 2.2%, 4.4%, and 2.5%, respectively.

Results

At the outset of this investigation, an inventory of collapse dolines was meticulously established. This inventory was based on a visual analysis of a set of aerial photographs, followed by on-site fieldwork. The outcome unveiled the presence of 32 collapse dolines within the study area. These dolines predominantly manifest in a NE–SW orientation (Fig. 2), aligning with the major fault direction as reported in previous studies (Boualla 2016; Boualla et al. 2021). The first identified collapse doline (**D1**) is located on the coastal cliff of the study area (Fig. 5). It significantly affects both the Plio-quaternary and the Upper Jurassic evaporitic complex formations. Further exploration of the identified collapse dolines was consistently conducted along the same NE–SW alignment (Fig. 2), revealing their relatively ancient age. Each of these identified dolines highlights the Quaternary formation as most vulnerable to collapse incidents, followed by the Plio-quaternary and the evaporitic complex formations. Moreover, in-depth investigations were conducted on the deeper dolines, with a specific focus on D21, D22, and D30. This internal exploration aimed to ascertain their lithological composition, depths, and the potential presence of structural features like faults and folds. In fact, this

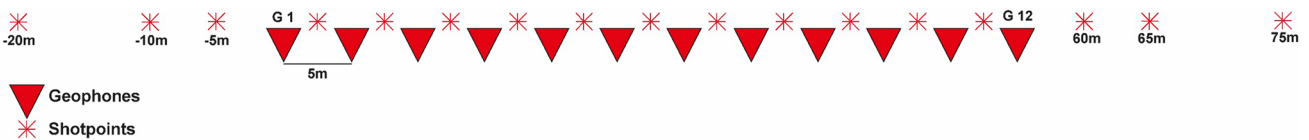


Fig. 3 Schematic illustration of the seismic refraction tomography acquisition process

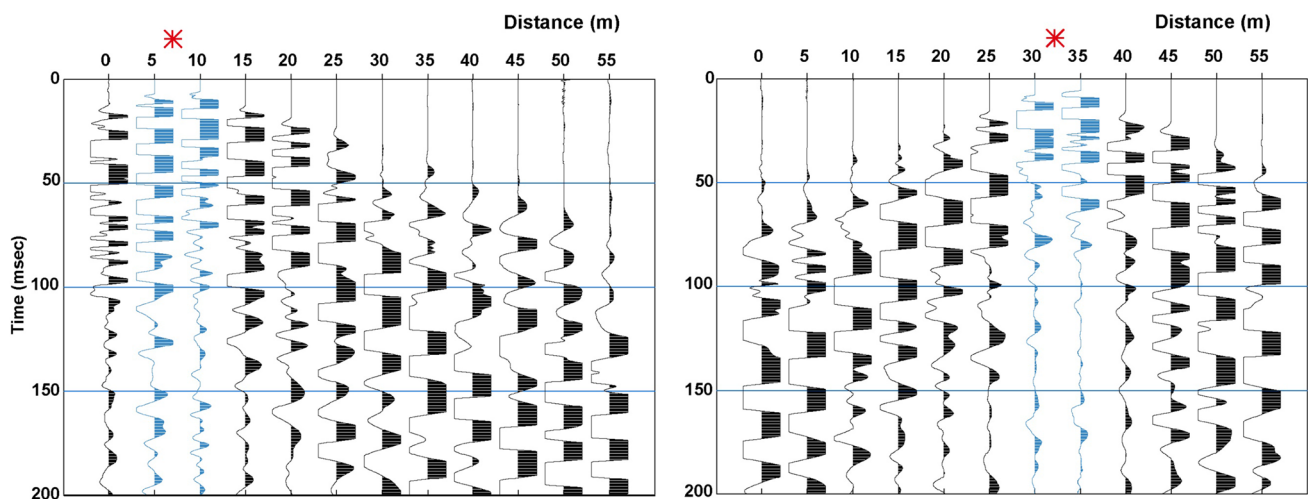


Fig. 4 Illustrations of P-wave arrival patterns in seismic sections acquired along the **SRT2** profile, corresponding to shotpoints at 7.5 m and 32.5 m

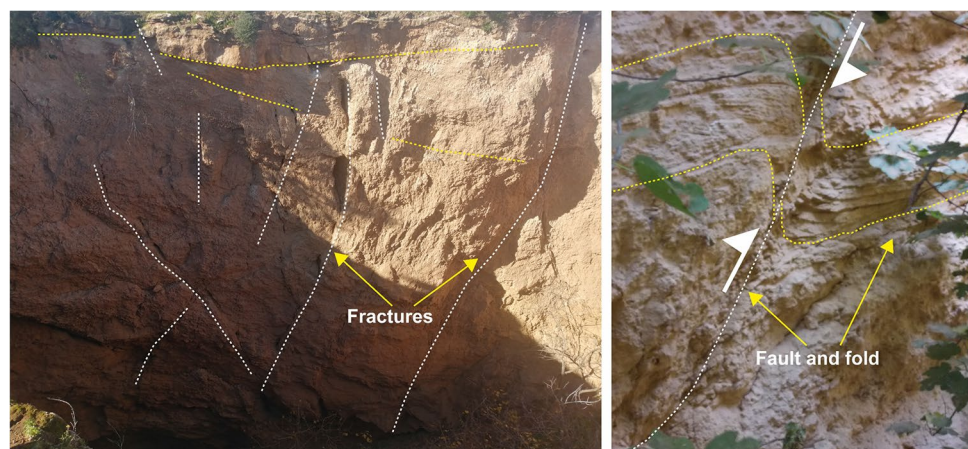


Fig. 5 Illustrative photos showing an example of collapse dolines inventoried across the study area: Dolines D1, D21, D22, D28, and D30

exploratory phase provided the essential basis for generating comprehensive geological cross sections, which were subsequently used to calibrate the geophysical profiles. The obtained results revealed the presence of fractures, faults, and folds within the walls of specific collapse dolines (Fig. 6). In addition, declarations of local landowners indicate that dolines **D28** and **D29** occurred around 1996 and 2014, respectively, due to heavy rainfall events. According to Boualla (2016), these periods registered exceptionally high levels of precipitation, with averages of 1018.9 mm in 1996 and 517.2 mm in 2014. Remarkably, parallel conclusions were drawn by Boualla et al. (2021) within the Moul El Bergui region to the north-east of the study area (Fig. 1). In their studies, conducted through aerial photography, Boualla

et al. (2016), 2021 indicates that the occurrence of these sinkholes can be traced back to 1962. Nevertheless, it's crucial to note that these dates are relative, and the majority of sinkholes lack precise dating. An effort to determine the age of a particular sinkhole yielded a result exceeding five thousand years, as reported by Weisrock and Lunski in 1987. The age-old existence of collapse dolines is evident in their physical characteristics. While certain collapse dolines exhibit steep, funnel-shaped walls, the majority have undergone erosion and sediment and boulder deposition, leading to less steep walls. Consequently, these on-site observations confirm that the collapses are influenced by tectonic factors, precipitation patterns, and the dissolution of gypsum and carbonate. In this work, the geological description will

Fig. 6 Example of karstic structures discovered within the wall of doline D21, white arrows indicate the direction of fault movement



exclusively involve the dolines located in close proximity to the geophysical profiles. Based on the field survey outcomes, the geophysical profiles were oriented in a mean N14 (N–S) direction, perpendicular to the doline alignment (Fig. 2). This orientation facilitates the detection of potential fault alignments that may be involved in the occurrence of these collapses.

Profile ERT1 was executed between the collapse dolines **D4** and **D5**, as indicated in Fig. 2. This profile shows a range of resistivity values fluctuating between 10 and more than 200 Ohm m (Fig. 7a). Notably, the profile surface exhibits a resistive level characterized by medium to high resistivity values, ranging from 30 to over 200 Ohm.m. In contrast, the deeper part of this profile reveals a conductive level, displaying a lower resistivity range of 10–<30 Ohm m. The geological calibration of this profile was based on the lithological section of the coastal cliff (Fig. 7b). The resistive level is assigned to the Plio-Quaternary formation, typically found at an average depth of 30 m. The upper part of this formation consists of sandstone and limestone, accounting for the evident resistivity heterogeneity. The subsequent geoelectric level with low resistivity corresponds to the lower part of the Pliocene layer, characterized by the presence of sandy and marly limestone. Interestingly, distinctive electrical

discontinuities emerge within this profile, particularly between 150 and 225 m where they intersect with D4 and D5, as well as at distance ranges of 50–80 m and 290–310 m. The first discontinuity, which is resistive (30–90 Ohm m) and extending to substantial depths, can potentially be attributed to the resistive collapsed materials constituting the roof of the dolines. This phenomenon is consistent with findings from previous studies using ERT (Nicod 1972; Youssef et al. 2012) that highlight the existence of resistant collapsed materials. Weisrock and Lunski (1987) observed that the collapse dolines within the study area are typically filled with Quaternary silts and dune materials. Furthermore, this discontinuity may signify a fault or fracture contributing to the collapse, potentially connecting to the Upper Jurassic layer. This prospect confirms the influence of the deep Jurassic karst on post-Pliocene superficial karst (Roch 1950; Weisrock and Lunski 1987). Similarly, the second geoelectric discontinuities with low resistivity, observed at depth intervals of 50–80 m and 290–310 m, may be indicative of the existence of additional faults or fractures associated with these ground movements.

Profile ERT2 was conducted between the collapse dolines D13 and D14, as depicted in Fig. 2. This profile reveals resistivity values ranging from 10 to 500 Ohm m

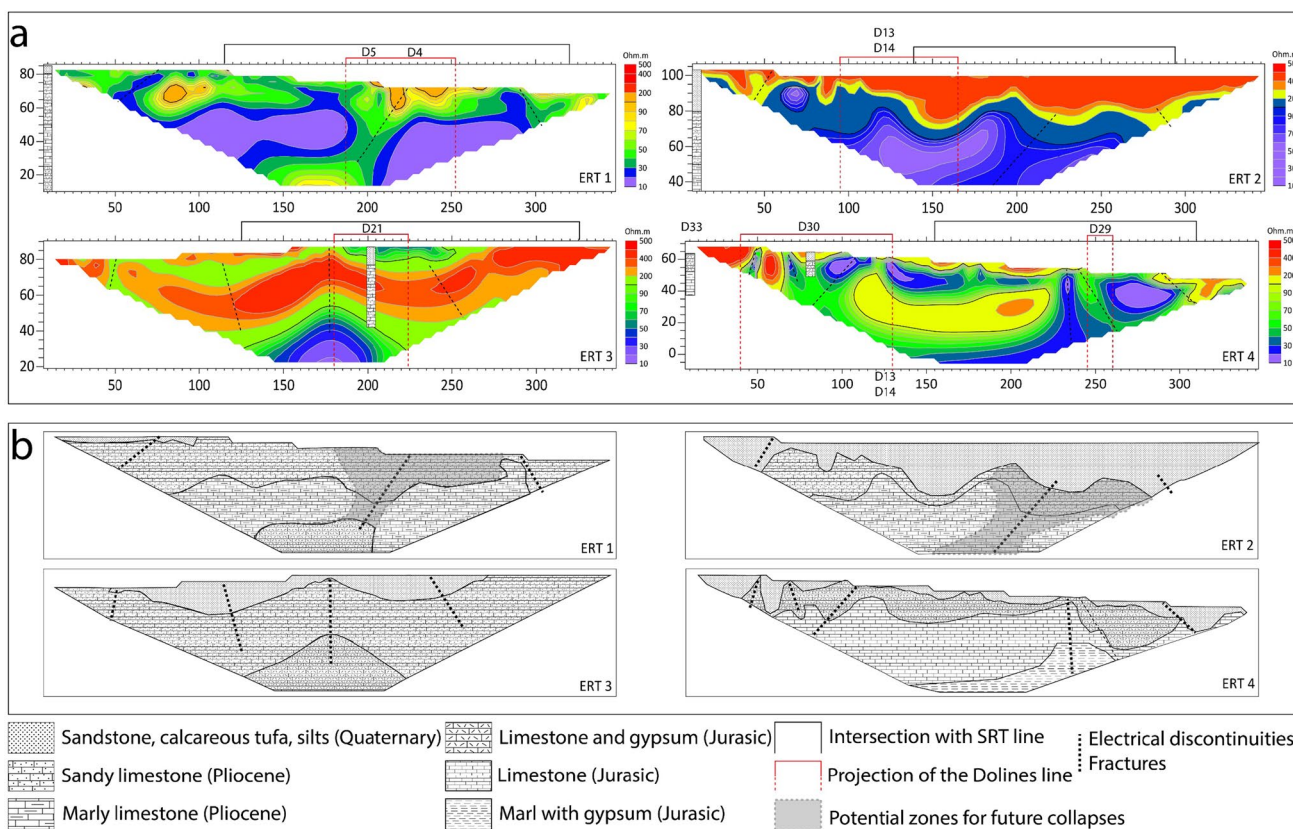


Fig. 7 Electrical resistivity tomography profiles: **a** inverted Profiles, **b** proposed geological Interpretation

(Fig. 7a). Within this range, resistivity values between 200 and 500 Ohm manifest as a distinct resistive level measuring around 10–20 m in thickness. This level corresponds to Quaternary sandstone and limestone. Subsequent to this, the profile transitions to a conductive level with resistivities between 10 and 90 Ohm m, aligning with the marly limestone formations of the Pliocene age (Fig. 7b). A noteworthy feature within this profile is the presence of several discernable discontinuities, with the most prominent one appearing at a distance between 180 and 225 m. Interestingly, this discontinuity is similar to that observed in ERT1 beneath D4 and D5. Consequently, this structural characteristic might delineate the boundaries of the collapsed zone and potentially represent a major fault line or fracture.

The execution of profile ERT3 took place along the western perimeter of the most profound collapse doline, D21, reaching a remarkable depth of 44 m (Figs. 2 and 5). This profile displays heterogeneous resistivities ranging from 10 to 500 Ohm m (Fig. 7a). A resistive level is observed in the center of the profile, exhibiting high resistivity values within the range of 200–500 Ohm m. This particular resistive level is attributed to the presence of sandstone and limestone from the Plio-quaternary age (Fig. 7b). A direct inspection of the walls of D21 revealed the presence of fractures with discernable relative movements among fractured blocks (Fig. 6). Moreover, the profile presents a conductive level at its surface, characterized by an average resistivity comprised between 70 and 200 Ohm m. This medium-resistivity level, extending approximately from 10 to 15 m in thickness, corresponds to the Quaternary sandstones, calcareous tufa and silts. Moving into deeper strata, another significant feature appears a conductive level characterized by low resistivities varying between 10 and 30 Ohm m. This specific segment is associated with the Jurassic gypseous layer. Like previous profiles, several electrical discontinuities are spotted along this profile, with the most pronounced ones emerging in proximity to D21 (at distances between 175 and 300 m), reflecting the presence of karstic faults or fractures. Interestingly, the lower boundary of D21 coincides perfectly with the conductive level attributed to the Jurassic gypsum. This observation justifies the fact that the cavity responsible for the occurrence of this doline exists within this formation.

In its turn, profile ERT4 was set in proximity to D29 and D30 (Figs. 2 and 7). Starting at the surface, a resistive level emerges with high resistivity values ranging from 200 to 500 Ohm m. As we delve deeper, another resistive level, with resistivity values ranging from 50 to more than 200 Ohm m, becomes apparent starting at a depth of 30 m. This second resistive level displays a notable increase in thickness compared to the first level. At an average depth of 30 m, a first conductive level emerges below the surface with resistivity values comprised between 10 and 50 Ohm m. Further down the profile, yet another conductive level appears at

a depth of 60 m, spanning resistivity values between 10 and 30 Ohm m. According to lithological observations made at D30, it becomes evident that the first resistive level detected at the surface is closely aligned with Plio-quaternary sandstone and limestone formations. However, the conductive level correlates significantly with the evaporitic complex. Remarkably, these geoelectric levels exhibit a series of sequential discontinuities, occurring at distances of 50, 65, 110, 240, and 280 m. These recurring discontinuities could potentially indicate the presence of faults or fractures. Moving deeper beneath D29, an intriguing phenomenon emerges as the conductive level intersects with a resistive one, whose shape is similar to the discontinuities encountered in both ERT1 and ERT2. Within this context, it is plausible to conclude that fractures promoted water infiltration, subsequently leading to the dissolution of limestone and gypsum. This process, in turn, contributed to the occurrence of dolines observed within these geological formations.

Building upon previous findings, SRT profiles were meticulously aligned with the electrical discontinuities detected on the ERT profiles around the identified dolines, as depicted in Fig. 2. Figure 8 shows all the first arrival times captured on the seismic sections, which were subsequently used for the tomographic inversion process. This figure clearly displays the variability in seismic wave arrival times across diverse profiles, primarily attributed to alterations in the facies and lithology of the study area. When examining the travel time curves for all the refraction data, we note that they appear quite disturbed and irregular, making it challenging to distinguish a specific delay pattern. However, we can identify some interesting variations in the initial breaks. Specifically, in SRT1, SRT3, and SRT4 profiles, a noticeable delay becomes apparent within the distance ranges of 0–110 m, 50–120 m, and 0–90 m, respectively. In contrast, the SRT2 profile shows a relatively consistent pattern of arrival times. This observed delay may potentially indicate the presence of cavities, fractures, faults, or other karst-related features. Based on these travel time curves and field results, the variations in velocity are consistent with the intersections of lines marking the known locations of the dolines (Fig. 2). Therefore, SRT models will be used to delineate the different velocity variations that may be related to karst structures.

Crossing D4 and D5, the SRT1 profile was aligned parallel to the ERT1 profile and extended for a length of 205 m (Fig. 2). The resulting model reveals a succession of three layers with average velocities varying between 0.5 and 2.3 km/s (Fig. 9a). The first layer exhibits velocities ranging from 0.5 to 0.9 km/s, with greater thickness observed within distances of 40 and 110 m, gradually thinning out along the rest of the profile. This variation can be explained by the presence of discontinuities at this level, causing wave deceleration and consequent changes in the formation thickness.

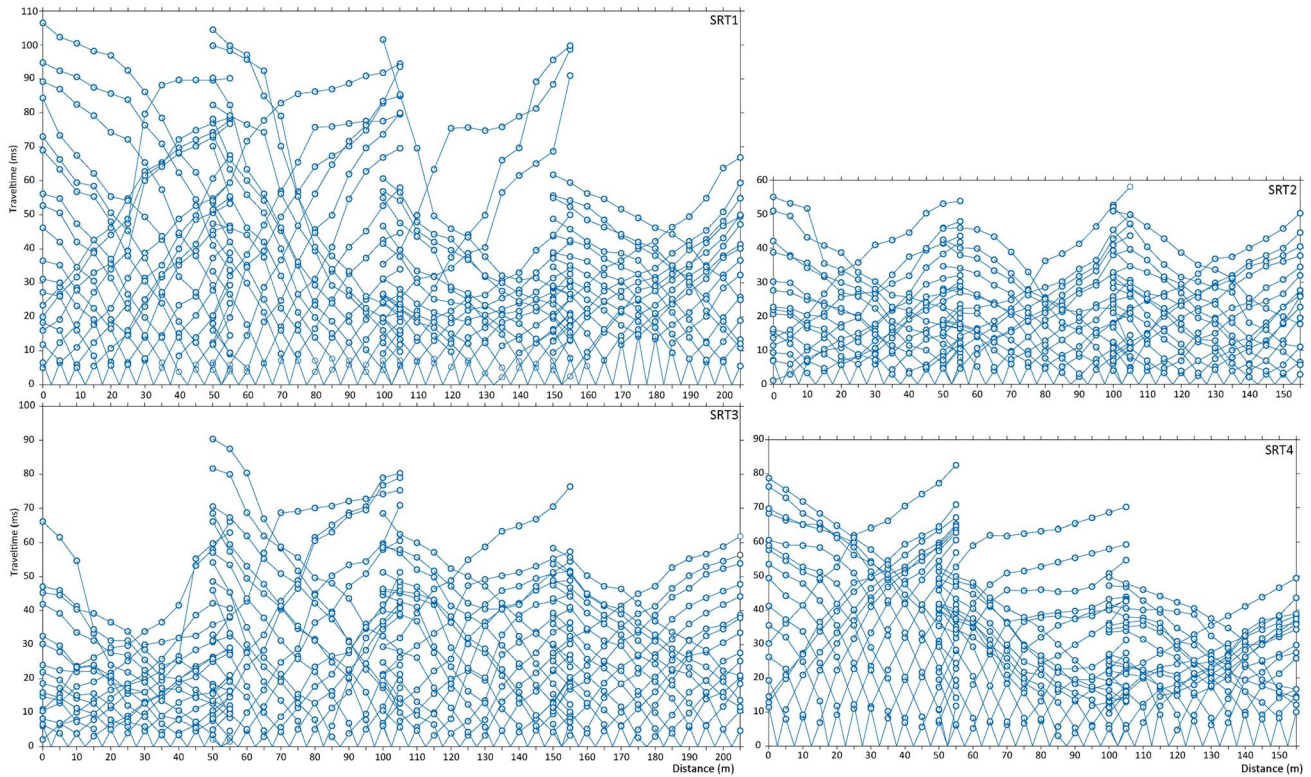


Fig. 8 Travel time–distance curves along Seismic Refraction Tomography profiles

Based on the lithology of the area's cliff (Fig. 9b), this first layer can be attributed to Quaternary sandstone. Regarding the second layer, it displays greater thickness compared to the first, featuring velocities ranging from 1.1 and 1.7 km/s. The thickness of this layer is variable and marked by seismic anomalies mainly emerging at distance ranges of 100–120 m and 180–200 m. The geological calibration allowed to attribute this layer to Pliocene sandy limestone. The last layer, characterized by velocities exceeding 1.7 km/s, maintains a relatively uniform thickness throughout the whole profile. This seismic layer is attributed to Pliocene marly limestone. As a result, this profile clearly highlights visible discontinuities in the first formations, which are successively located within distance ranges of 100–120 m and 180–200 m. In a broader context, the observed changes in velocity are primarily linked to the presence of fractures within the formation, which affects both travel time and amplitude of seismic waves. Furthermore, these changes could suggest the potential presence of a cavity, leading to a slowdown of seismic waves, especially within the distance range of 20–110 m. Crossing the discontinuity recorded at a distance of 110 m, the change in velocity becomes more pronounced, which is consistent with the alignment of D4 and D5 (Fig. 9).

Aligned with ERT2, the SRT2 profile was positioned to pass through D12 and D13, covering a distance of 155 m (Fig. 2). This profile also exhibits average velocities ranging

from 0.5 to 2.3 km/s, with a three-layer model. With insignificant variations, the thicknesses of the seismic layers are relatively uniform, as displayed in Fig. 9a. The first layer shows velocities between 0.5 and 0.9 km/s while maintaining a relatively consistent thickness varying between 1 and 1.5 m. The second layer displays velocities in the range of 1.1–1.9 km/s and a thickness varying from 3 to 15 m. Whereas, the last highlighted formation (3rd layer) showcases velocities exceeding 1.9 km/s. In line with the seismic and geological analysis of SRT1, the first and second layers in this profile correspond respectively to Quaternary sandstone and Pliocene sandy limestone (Fig. 9b). The SRT2 profile also unveils two seismic discontinuities less significant compared to those observed in SRT1. The first emerges around a distance of 40 m, followed by the second closer to a distance of 95 m. Although the velocity change within the first discontinuity is insignificant, its alignment with the position of the dolines implies the potential presence of fractures or faults.

The SRT3 was established in close proximity to D21, over a distance of 205 m. The inverted model also presents a three-layer succession, with average velocities ranging from 0.5 to 2.3 km/s (Fig. 9a). Despite being relatively thin, the thickness of the first two layers notably expands within the distance range of 40–120 m. Within this range, the profile shows two main seismic discontinuities distinguished

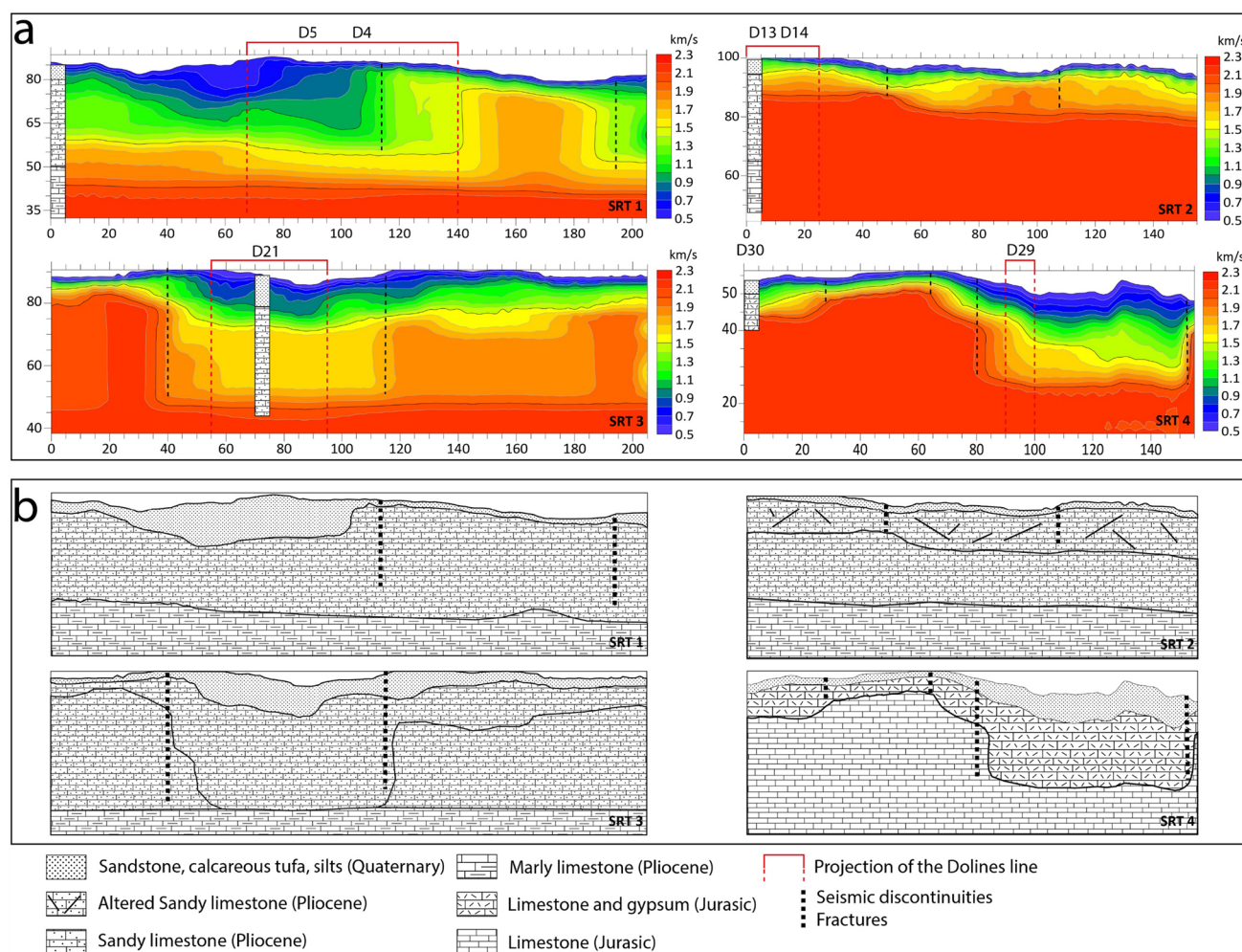


Fig. 9 Seismic refraction tomography profiles: **a** inverted Profiles, **b** geological Interpretation

respectively at distances of 40 and 110 m. It should be noted that the midpoint of this range aligns perfectly with the projection of D21 onto the profile. This alignment supports the fact that these anomalies may indeed correlate with faults or fractures that contribute to the velocity changes in this specific part of the profile. The first layer, characterized by a slower velocity ranging from 0.5 to 0.9 km/s and a moderate thickness, is attributed to Quaternary sandstone and calcareous tufa (Fig. 9b). On the other hand, with velocities varying between 1.1 and 1.9 km/s and an increasing thickness within the range of 40–110 m, the second layer is attributed to Pliocene sandy limestone.

The SRT4 profile shows the same sequence of seismic layers observed in the previous profiles (Fig. 9). Additionally, seismic discontinuities are clearly discernable on this profile, appearing successively within the distance ranges of 25–65 and 80–150 m. Interestingly, the seismic anomaly at a distance of 80 m is marked by an increase in the thickness of the first formation, matching findings from the STR3 profile.

This discontinuity may correspond to a fracture or an underground cavity, as it coincides with a decrease in seismic wave velocities. The first layer, of 0.5–0.9 km/s and an average thickness of 5–10 m, is attributed to Quaternary sandstone and limestone. The second layer is characterized by velocities ranging between 1.1 and 1.9 km/s and an increasing thickness around the seismic discontinuity located at 60 m. This layer is attributed to Pliocene sandy limestone. With velocities exceeding 1.9 km/s, the third layer is thought to be a Jurassic gypseous layer.

In general, the geophysical profiles obtained through both ERT and SRT techniques revealed a series of distinct discontinuities. The unique characteristic of these anomalies resides in their correlation with the dolines identified in the field. Therefore, they could serve as valuable indicators of potential karstic fractures or faults. Operating as pathways for both surface and subsurface water drainage and flow, these fractures facilitate water circulation, expediting the dissolution of carbonates and gypsum. This mechanism

ultimately governs the existence and genesis of the collapse dolines, thereby influencing their occurrence patterns.

Discussions

The primary objective of this study was to explore the processes and mechanisms contributing to the formation of collapse dolines in the Abda region of western Morocco. This investigation employed an integrated approach, incorporating fieldwork, geological studies, and geophysical survey. The results revealed the existence of over thirty collapse dolines in the research area. These dolines were primarily oriented in the NE–SW direction following major fault lines. Field observations yielded valuable insights into the composition and age of these dolines, offering information on the susceptibility of various geological formations to collapse events. Notably, the Quaternary formation exhibited the highest vulnerability, followed by the Plio-Quaternary formations and the evaporitic complex. Furthermore, geophysical findings indicate the existence of structural anomalies, which are interpreted as faults or fractures. These geological structures contribute to the spatial occurrence of collapse dolines.

The field investigation results revealed a prevalence of collapse dolines within the study area, predominately aligned along a NE–SW orientation. This is consistent with the study conducted by Boualla (2016), which covered the entire Abda region and identified a concentration of collapse dolines exclusively in the southern vicinity of Safi city. Boualla et al. (2016) further linked this distribution to prominent predisposing factors found in this area, including lithological variations, topographical characteristics, and structural elements. These factors are exacerbated by human activities, primarily through the practice of agricultural irrigation (Boualla et al. 2021). Notably, the study area exhibits a dual karstic nature: a deep karst formed by alternating layers of limestone, marl, and gypsum, alongside a superficial karst rich in bioclastic limestone (Roch 1950; Gigout 1951; Weisrock and Lunski 1987). The presence of the evaporitic complex formation, enriched with gypsum and anhydrite, is believed to significantly contribute to the occurrence of numerous dolines due to its susceptibility to rapid dissolution. Additionally, the distribution pattern of the identified collapse dolines aligns with the potential presence of flexures, faults, and folds in the research area (Boualla 2016; Bouzerda et al. 2020; Boualla et al. 2021). This alignment suggests a substantial correlation between tectonic structures and the occurrence of dolines, particularly along faults and fractures. Supporting this hypothesis, speleological exploration of certain deep dolines revealed the existence of tectonic features, including folds, fractures, and faults (Fig. 6).

The combined implementation of ERT and SRT techniques yielded invaluable insights into the diverse characteristics of this karstic landscape. The obtained results revealed that the karstic features of the region are influenced by several discontinuities, identified as faults or fractures. The deliberate positioning of the geophysical profiles to cross the dolines proved to be effective. Therefore, elucidating a clear convergence between the identified discontinuities and the doline's line. This correlation is visually depicted in Fig. 10, presenting a comparative juxtaposition of ERT and SRT profiles. A thorough analysis indicates remarkable similarities between the discontinuities identified by these two methods. These similarities are particularly apparent in ERT1-SRT1, ERT2-SRT2, and ERT4-SRT4 comparisons. For instance, the comparison between ERT2 and SRT2 shows more or less consistent resistivities and velocities, suggesting the existence of relatively uniform layers. The characteristics and locations of these discontinuities, which match the projection of the collapse dolines, suggest a fairly reliable interpretation. Taking into account the field observations, SRT surveys proved to be a valuable tool for confirming the results obtained by ERT. It should be noted that conventional refraction techniques may encounter challenges in detecting cavities, which are typically marked by a decrease in velocity (Cardarelli et al. 2010; Amanatidou et al. 2022).

In this study, the average velocity of seismic wave propagation remained within the characteristic range of solid formations. However, in profiles SRT1 and SRT4, low-velocity anomalies successively intersecting with D4 and D29 can be detected. This finding is potentially indicating the presence of probable cavities. Interestingly, these discontinuities align with resistive discontinuities in profiles ERT1 and ERT4 (Fig. 10). Although the velocity values do not precisely correspond to the expected air velocity of 0.3 km/s (Amanatidou et al. 2022). However, the decrease is clearly noticeable across these profiles. This phenomenon, commonly encountered in karstic studies, highlights the inherent challenge of accurately deducing the presence of cavities through inversion processes (Amanatidou et al. 2022). Conversely, the resistive discontinuity beneath D21 observed in ERT3 corresponds to a progressive velocity increase in SRT3 (Fig. 10). This result suggests the existence of a massive limestone formation. Therefore, the geophysical discontinuities detected in both ERT and SRT profiles can be broadly interpreted as faults or fractures.

Overall, the geophysical findings revealed the presence of structural anomalies in the study area. These latter were interpreted especially as faults or fractures. These anomalies provide compelling reasons for the likelihood of spatial occurrence of collapse dolines. Consequently, the potential for collapse persists as long as additional triggering factors, such as precipitation and anthropogenic influences, remain steady and do not surpass specific thresholds (Boualla et al.

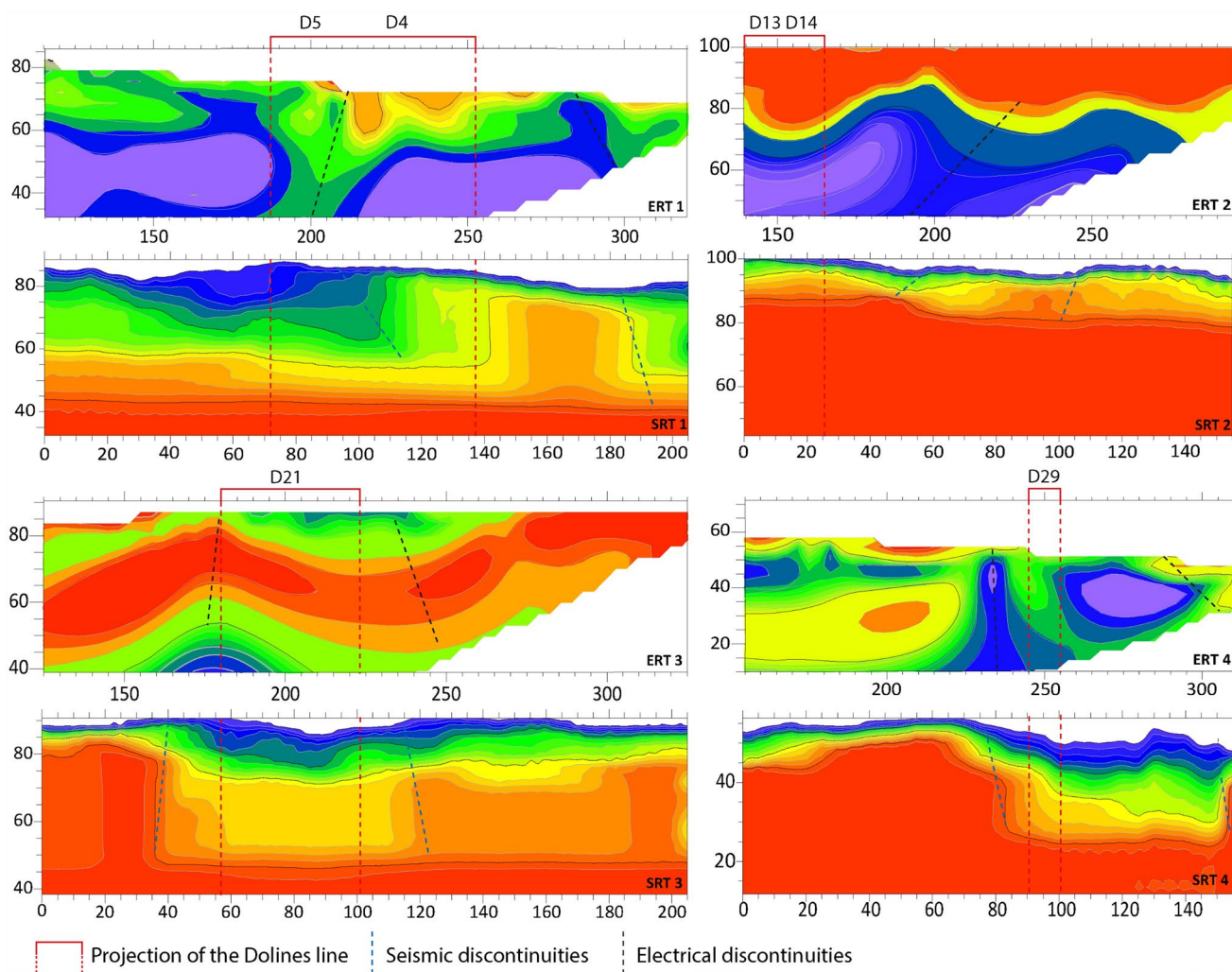


Fig. 10 Comparative analysis of electrical resistivity tomography and seismic refraction tomography profiles with equal dimensions

2016). For instance, substantial rainfall alone is sufficient to trigger or reactivate the occurrence of collapse dolines in this area. In addition, the combination of ERT and SRT profiles not only offers a powerful predictive tool for collapses in the near or distant future but also sheds light on their spatio-temporal evolution. This spatio-temporal aspect, promoted by 2D visualization, substantially enhances the accuracy of dolines susceptibility mapping (Boualla et al. 2016). However, the geophysical survey is not limited to imaging anomalies associated with collapse dolines. This method can also predict the spatio-temporal probability of occurrence by visualizing the collapsing structures.

Lineaments are typically linear features serving as visual indicators of geological structures. These features can include a variety of geological elements, such as faults, joints, and fractures (Habib et al. 2013; Theilen-Willige et al. 2014; Bouazama et al. 2023). Using this method can provide reliable evidence about the geological evolution and

structural composition of the surveyed region. Accordingly, a thorough investigation of the lineaments was carried out in the study area to further confirm the geophysical findings. This investigation was based on data from the Advanced Land Observing Satellite (ALOS) and the Shuttle Radar Topography Mission (SRTM). Digital Elevation Models (DEM) covering the study area were downloaded for free from the official websites of NASA (earthdata.nasa.gov, 2023) and the USGS (earthexplorer.usgs.gov, 2023), with spatial resolutions of 12.5 m and 30 m, respectively. Subsequently, lineaments were extracted using both manual and automatic methods, following the steps outlined in Habib et al. (2013), Enoh et al. (2021), and Villalta Echeverria et al. (2022). The extracted lineaments yielded a Kernel density map that represent their distribution across the study area (Fig. 11).

In a geological context, the density of the lineaments is commonly used as an indicator of the degree of fracturing

of the rock, with higher densities reflecting areas of strong fracturing. The obtained results show that the density of lineaments is very high to the south and moderate to very low to the north of the study area. Remarkably, the boundary between these two zones corresponds perfectly to the alignment of the collapse dolines. Moreover, the analysis of the rose diagram illustrating the distribution of lineaments shows predominant orientations along the NE–SW direction (Fig. 11). This orientation is consistent with the prevailing alignment of the major faults encountered in the study area. In accordance with this, Bouazama et al. (2023) highlighted several morphological lineaments between Safi and Oualidia, preferentially aligning from NNE–SSW to NE–SW. They claimed that the distribution of these lineaments is strongly linked to tectonic events, implying a series of complex subsurface structures such as faults, fold axes, or both. Consequently, the results obtained from the distribution of lineaments confirm the geophysical findings. Therefore, it can be concluded that the collapse dolines follow a faults line, which represent a weakness plane and also promotes the infiltration and circulation of water. This latter will, therefore, accelerate the dissolution process of limestone and evaporite encountered in the study area.

The overall outcomes of this study firmly establish the presence of karstic features within the surveyed area. These features appear as Plio-quadernary sandstone and limestone formations in the superficial karst, while they manifest as underlying Jurassic marly limestone and gypsum formations within the deep karst. Notably, these formations are the most susceptible to dissolution processes. In locations where the fracturing phenomenon prevails, these karstic features become more exposed to water infiltration that promotes the dissolution of carbonate and gypseous layers. Over time, this process gradually expands the fractures and spreads the underground karstic networks, stimulating the genesis of more cavities. In fact, the continual erosion of the subsoil subsequently leads to a progressive weakening of the ground surface. This ultimately results in the ground subsidence into the formed cavities. As demonstrated previously, the occurrence of collapse dolines in the study area firmly follows the alignment of faults and fractures. According to Boualla et al. (2021), their occurrence is also due to several predisposing factors, including topography, geological structure, hydrology, and climatic conditions. Synthesizing the findings of both the current study and previous research, it becomes evident that regions sharing similar characteristics with the Abda region are susceptible to a substantial risk for

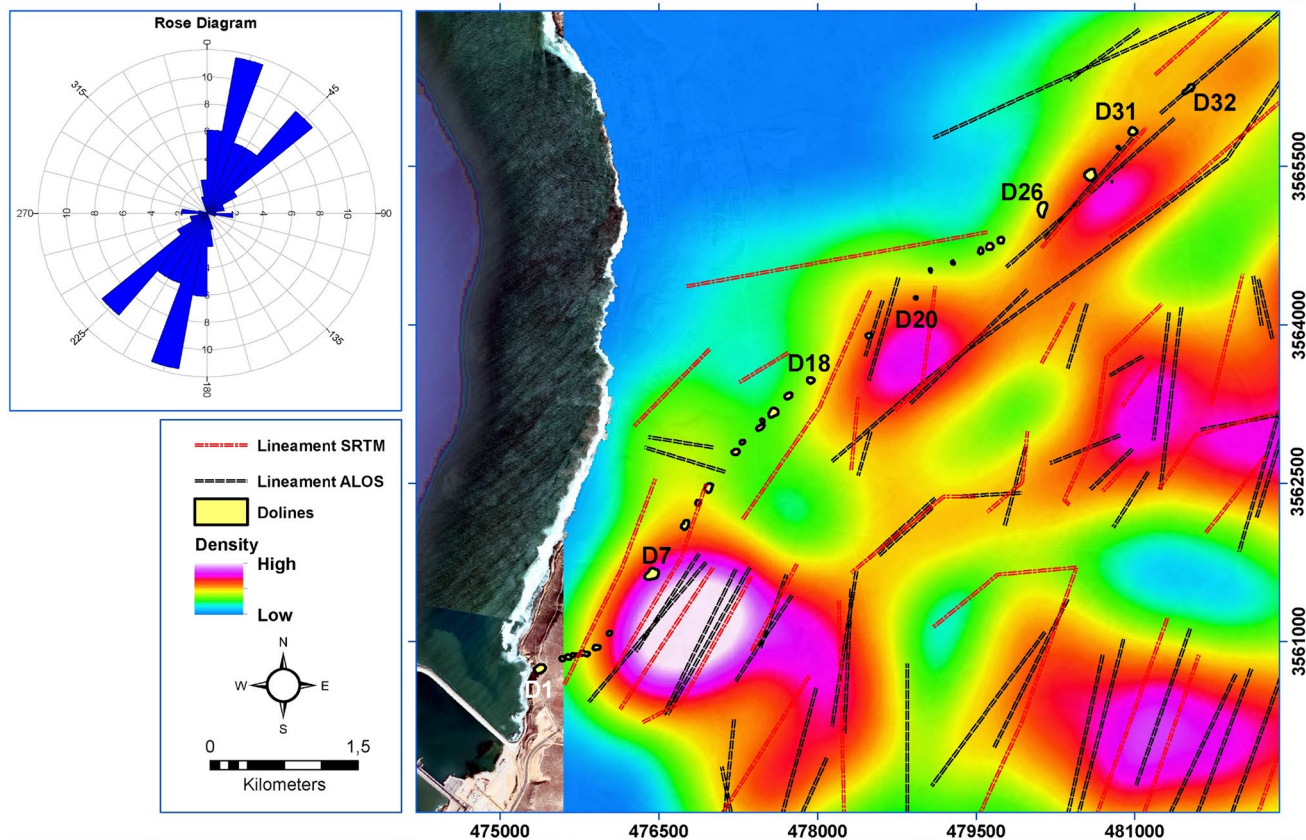


Fig. 11 Lineament density map of the study area

collapse. This susceptibility is due to the simultaneous convergence of factors such as fracturing, the presence of carbonate or evaporite formations, and topographic variations. To effectively mitigate the associated risks, a comprehensive regional assessment is recommended. This assessment should include an exhaustive mapping aimed at delineating the distribution and interrelationships of these factors across the entire region.

Conclusion

This study systematically investigated the processes and mechanisms of the genesis of collapse dolines within the Abda region in western Morocco. This investigation was based on an integrated approach combining fieldwork, geological survey, and geophysical techniques. The results unveiled a notable presence of more than thirty collapse dolines, which are predominantly oriented in a NE–SW direction. This direction follows the alignment of major faults identified in previous studies within the study area. The found alignment highlighted the relationship between tectonic features and the occurrence of dolines.

The field observations provided valuable insights into the composition and age of the collapse dolines. Each doline provides information about the susceptibility of different geological formations to collapse events. Notably, the Quaternary formation displayed the highest vulnerability, followed by the Plio-quaternary and evaporitic complex formations. The integration of ERT and SRT techniques yielded further geological understanding. The geophysical profiles identified anomalies that coincided with the locations of the collapse dolines, indicating potential faults and fractures. This correlation reinforces the close relationship between structural elements and the occurrence of dolines. The findings of this study align with prior research, emphasizing the role of lithology, topography, and tectonic structures in dictating the distribution of collapse dolines. Particularly, the presence of gypsum and carbonate formations significantly heightened the susceptibility to dissolution processes. Moreover, the analysis of the density map of lineaments confirmed the alignment of the dolines with major faults and subsurface structures.

Overall, the convergence of ERT and SRT profiles with geological characteristics, coupled with the alignment of dolines with tectonic features, stresses the robustness of the findings. The study highlights that the susceptibility of the Abda region to collapse events is driven by a combination of geological composition, structural elements, and hydrological patterns. These factors collectively amplify the risk of surface subsidence due to continual erosion and dissolution processes. To effectively manage these risks, it is recommended to initiate an exhaustive mapping with meticulous

delineation of influential factors across the entire region. Furthermore, areas that have experienced collapse can be indicative of potential underground cavities. Consequently, it is advisable to map these regions utilizing regional geophysical methods. Hence, to mitigate the substantial impact of this phenomenon, identifying the diverse causal factors of such collapses will facilitate the development of a comprehensive risk map within the area. This proactive approach will provide a solid foundation for informed decision-making and risk mitigation strategies, ultimately ensuring the safety and stability of vulnerable areas. Given this in-depth understanding, it is crucial to consider the potential risks of sinkhole collapse in regions exhibiting similar characteristics to those of the study area. Therefore, the findings of this study are not limited to the Abda region; rather, they are applicable to all regions with comparable geological features.

Declarations

Conflict of interest The authors declare that they have no known competing financial interests or personal relationships that could have appeared to influence the work reported in this paper.

References

- AlQahtani HH, Fnais MS, Almadani SA, Alhumimidi MS, Abdelrahman K (2021) Electrical resistivity and refraction seismic tomography in the detection of near-surface Qadimah Fault in Thuwal-Rabigh area, Saudi Arabia. *Arab J Geosci* 14:1–9
- Amanatidou E, Vargemezis G, Tsourlos P (2022) Combined application of seismic and electrical geophysical methods for karst cavities detection: a case study at the campus of the new University of Western Macedonia, Kozani, Greece. *J Appl Geophys* 196:104499
- Ammar AI, Kamal KA (2018) Resistivity method contribution in determining of fault zone and hydro-geophysical characteristics of carbonate aquifer, eastern desert, Egypt. *Appl Water Sci* 8:1–27
- Boualla O, Mehdi K, Zourarah B (2016) Collapse dolines susceptibility mapping in Doukkala Abda (Western Morocco) by using GIS matrix method (GMM). *Model Earth Syst Environ* 2(1):9
- Boualla O, Fadili A, Najib S, Mehdi K, Makan A, Zourarah B (2021) Assessment of collapse dolines occurrence using electrical resistivity tomography: case study of Moul El Bergui area, Western Morocco. *J Appl Geophys* 191:104366
- Boualla O (2016) Etude des risques de mouvements de terrain dans la région de SAFI (Maroc). In: *Approche géomatique, géophysique et géostatistique (Thèse de Doctorat)*, Université Chouaïb Doukkali El Jadida, p 347
- Bouazama I, Bba AN, Aabi A, Hejja Y, Moua SO, Baïdler L, Manar A (2023) The role of structural inheritance in the tectonic configuration of the Moroccan Meseta Coastal Block: insights from morpho-structural and aeromagnetic data. *J Afr Earth Sci*. <https://doi.org/10.1016/j.jafrearsci.2023.104978>
- Bouzerda M, Mehdi K, Fadili A, Boualla O (2020) Collapse dolines susceptibility mapping using frequency ratio method and GIS in Sahel-Doukkala, Morocco. *Model Earth Syst Environ* 6(1):349–362
- Cardarelli E, Cercato M, Cerreto A, Di Filippo G (2010) Electrical resistivity and seismic refraction tomography to detect buried cavities. *Geophys Prospect* 58(4):685–695

- Cardarelli E, Cercato M, De Donno G (2014) Characterization of an earth-filled dam through the combined use of electrical resistivity tomography, P-and SH-wave seismic tomography and surface wave data. *J Appl Geophys* 106:87–95
- Carollo A, Capizzi P, Martorana R (2020) Joint interpretation of seismic refraction tomography and electrical resistivity tomography by cluster analysis to detect buried cavities. *J Appl Geophys* 178:104069
- Choubert G, Faure-Muret A (1962) Evolution du domaine atlasique marocain depuis les temps paléozoïques. Livre à la mémoire du professeur Fallot P. *Mém Hors-Série Soc Géol France* 1:447–525
- De Giorgi L, Leucci G (2014) Detection of hazardous cavities below a road using combined geophysical methods. *Surv Geophys* 35:1003–1021
- Ducut JD, Alipio M, Go PJ, Concepcion R II, Vicerra RR, Bandala A, Dadios E (2022) A review of electrical resistivity tomography applications in underground imaging and object detection. *Displays* 73:102208
- Enoh MA, Okeke FI, Okeke UC (2021) Automatic lineaments mapping and extraction in relationship to natural hydrocarbon seepage in Ugwueme, South-Eastern Nigeria. *Geod Cartogr* 47(1):34–44
- Ferré M, Ruhard JP (1975) Ressources en eau t. 2, (Plaines et bassins du Maroc atlantique); les bassins des Abda-Doukkala et du Sahel d'Azemmour à Safi. *Not Mém Serv Géol Maroc* 231:261–298
- Gigout M (1951) Etudes géologiques sur la Meseta marocaine occidentale (arrière-pays de Casablanca, Mazagan et Safi). Travaux de l'Institut Scientifique Chérifien no 3, et notes et mémoires du Service géologique. No 86. Rabat, Imprimerie Maroc-Matin, 2 tomes; t. 1: 507 pp., 65 figures et t. 2: 18 planches de photographies, 9 planches de cartes et figures hors texte, 1 tableau
- Gilli É, Mangan C, Mudry J (2012) Hydrogéologie: objets, méthodes, applications, 3rd edn. Dunod, Paris, p 340
- Gómez-Ortiz D, Martín-Crespo T (2012) Assessing the risk of subsidence of a sinkhole collapse using ground penetrating radar and electrical resistivity tomography. *Eng Geol* 149:1–12
- Guedes VJCB, Borges WR, da Cunha LS, Maciel STR (2023) Characterization of an earth dam in Brazil from seismic refraction tomography and multichannel analysis of surface waves. *J Appl Geophys* 208:104893
- Gutiérrez Elorza M (2008) *Geomorfología*. Pearson, Madrid
- Habib A, Labbassi K, Akdim N, Tadj A (2013) Contribution des données Alos et Landsat dans la cartographie et l'analyse des linéaments dans le Sahel Central (Maroc occidental). *Revue Française De Photogrammétrie Et De Télédétection* 203:33–42
- Imposa S, Grassi S, Di Raimondo S, Patti G, Lombardo G, Panzera F (2018) Seismic refraction tomography surveys as a method for voids detection: an application to the archaeological park of Cava Ispica, Sicily, Italy. *Int J Archit Herit* 12(5):806–815
- Intrieri E, Confuorto P, Bianchini S, Rivolta C, Leva D, Gregolon S, Fanti R (2023) Sinkhole risk mapping and early warning: the case of Camaiole (Italy). *Front Earth Sci* 11:1172727
- Khoshlahjeh Azar M, Hamedpour A, Maghsoudi Y, Perissin D (2021) Analysis of the deformation behavior and sinkhole risk in Kerdabad, Iran using the PS-InSAR method. *Remote Sens* 13(14):2696
- Loke MH (2014) Tutorial: 2-D and 3-D electrical imaging surveys. Geotomo Software Company
- Loke MH, Barker RD (1996) Rapid least-squares inversion of apparent resistivity of pseudosections by a quasi-Newton method. *Geophys Prospect* 44:131–152
- Metwaly M, AlFouzan F (2013) Application of 2-D geoelectrical resistivity tomography for subsurface cavity detection in the eastern part of Saudi Arabia. *Geosci Front* 4(4):469–476
- Nicod J (1972) Pays et paysages du calcaire, Paris, collection, Sup, Le géographe, PUF, p 224
- Oliver-Cabrera T, Wdowinski S, Kruse S, Robinson T (2020) InSAR Detection of localized subsidence induced by sinkhole activity in suburban West-Central Florida. *Proc Int Assoc Hydrol Sci* 382:155–159
- Olivier G, De Wit T, Brenguier F, Bezuidenhout L, Kunjwa T (2018) Ambient noise love wave tomography at a gold mine tailings storage facility. *Geotech Lett* 8(3):178–182
- Pothérat P, Doridot M, Chahine M (1999) L'utilisation de la photo-interprétation dans l'établissement des plans de prévention des risques liés aux mouvements de terrain, Guide Technique, Collection environnement: les risques naturels, Paris, Edition du Laboratoire Central des Ponts et Chaussées, p 128
- Rizzo E, Giampaolo V, Capozzoli L, Grimaldi S (2019) Deep electrical resistivity tomography for the hydrogeological setting of Muro Lucano Mounts Aquifer (Basilicata, Southern Italy). *Geofluids*. <https://doi.org/10.1155/2019/6594983>
- Roch E (1950) Histoire stratigraphique du Maroc, Notes et mémoires du Service Géologique no 80 Les Frères. Toulouse, DOU-LADOURE, p 435
- Theilen-Willige B, Malek HA, Charif A, El Bchari F, Chaïbi M (2014) Remote sensing and GIS contribution to the investigation of karst landscapes in NW-Morocco. *Geosciences* 4(2):50–72
- Villalta Echeverria MDP, Viña Ortega AG, Larreta E, Romero Crespo P, Mulas M (2022) Lineament extraction from digital terrain derivative model: a case study in the Girón-Santa Isabel basin. *South Ecuad Remote Sens* 14(21):5400
- Weisrock A, Lunski S (1987) Le karst pliocène de la région de Safi (Maroc atlantique). *Karstologia* 9:31–36
- Williams PW (2003) Dolines. In: Gunn J (ed) encyclopedia of caves and karst science. Taylor & Francis e-Library, New York, pp 628–642
- Witam O (1988) Etude stratigraphique et sédimentologique de la série mésozoïque du bassin de Safi, action intégré 86–210. In: Mémoire no 3 Thèse de Doctorat de 3ème Cycle, Faculté des Sciences, p 194, Marrakech
- Youssef AM, El-Kaliouby HM, Zabramawi YA (2012) Integration of remote sensing and electrical resistivity methods in sinkhole investigation in Saudi Arabia. *J Appl Geophys* 87:28–39

Springer Nature or its licensor (e.g. a society or other partner) holds exclusive rights to this article under a publishing agreement with the author(s) or other rightsholder(s); author self-archiving of the accepted manuscript version of this article is solely governed by the terms of such publishing agreement and applicable law.